Available online at www.sciencedirect.com
SCIENCE DIRECT®
Bioorganic & Medicinal Chemistry 12 (2004) 3871–3883
Bioorganic & Medicinal Chemistry

Synthesis and biological evaluation of novel curcumin analogs as anti-cancer and anti-angiogenesis agents

Brian K. Adams,[a,b,e,†] Eva M. Ferstl,[b,†] Matthew C. Davis,[b] Marike Herold,[b] Serdar Kurtkaya,[b] Richard F. Camalier,[c] Melinda G. Hollingshead,[c] Gurmeet Kaur,[c] Edward A. Sausville,[c] Frederick R. Rickles,[d] James P. Snyder,[b,*] Dennis C. Liotta[b] and Mamoru Shoji[a,*]

[a]*Winship Cancer Institute, Emory University, Atlanta, GA 30322, USA*
[b]*Department of Chemistry, Emory University, Atlanta, GA 30322, USA*
[c]*Developmental Therapeutics Program, DCTD, NCI-Frederick, Frederick, MD 21702, USA*
[d]*Departments of Medicine and Pediatrics, The George Washington University School of Medicine and Health Sciences, Washington, DC 20037, USA*
[e]*Program in Molecular and Systems Pharmacology, Emory University, USA*

Received 28 January 2004; accepted 3 May 2004
Available online 5 June 2004

Abstract—A series of novel curcumin analogs were synthesized and screened for anti-cancer and anti-angiogenesis activities at Emory University and at the National Cancer Institute (NCI). These compounds are symmetrical α,β-unsaturated and saturated ketones. The majority of the analogs demonstrated a moderate degree of anti-cancer activity. Compounds **10**, **11**, and **14** exhibited a high degree of cytotoxicity in the NCI in vitro anti-cancer cell line screen. In addition, this screen revealed that these compounds inhibit tumor cell growth with a higher potency than the commonly used chemotherapeutic drug, cisplatin. In independent in vitro screens conducted at Emory, the same compounds plus **4**, **5**, **8**, **9**, and **13** exhibited a high degree of cytotoxicity to tumor cells. Analogs that were effective in the anti-cancer screens were also effective in in vitro anti-angiogenesis assays. Compounds **4**, **9**, **11**, and **14** were most effective in the anti-angiogenesis assays run at Emory. In the assays conducted by the NCI, compound **14** was almost as potent as the anti-angiogenic drug TNP-470, which has undergone clinical trials. Based on the favorable in vitro anti-cancer and anti-angiogenesis results with **14**, further in vivo tests were conducted. This compound effectively reduced the size of human breast tumors grown in female athymic nude mice and showed little toxicity. This data, coupled with the remarkable in vitro data, suggests that compound **14** may potentially be an effective chemotherapeutic agent. As a follow-up, a 3D quantitative structure relationship based on **14** has been developed. It shows a cross-validated $r^2(q^2) = 0.83$ and a predictive $r^2(p^2) = 0.71$. COMPARE analysis suggests the compound to be a possible RNA/DNA antimetabolite, but also implies that the compound's cytotoxicity may arise from a presently unknown mechanism.

1. Introduction

Curcumin (diferuloylmethane) **1** (Chart 1) is a β-diketone constituent of the turmeric that is obtained from the powdered root of *Curcuma longa* Linn. It is used as a spice to give a specific flavor and yellow color to curry, which is consumed daily by millions of people. Curcumin has been used by traditional medicine for liver

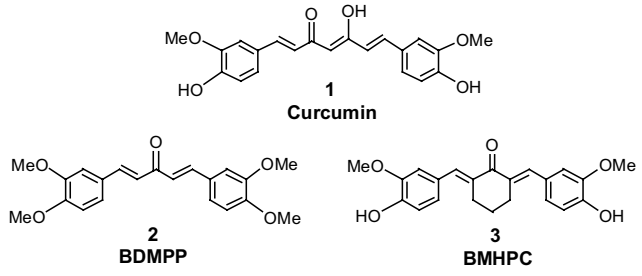

Chart 1.

Keywords: Synthetic curcumin analogs; Anti-cancer agent in vitro and in vivo; Anti-angiogenesis properties; 3D quantitative structure relationship (QSAR).
* Corresponding authors. Tel.: +1-404-727-2415; fax: +1-404-727-6586; e-mail: snyder@euch4e.chem.emory.edu
† These authors contributed equally in the writing of this manuscript.

0968-0896/$ - see front matter © 2004 Elsevier Ltd. All rights reserved.
doi:10.1016/j.bmc.2004.05.006

disease (jaundice), indigestion, urinary tract diseases, rheumatoid arthritis, and insect bites. This phytochemical has also demonstrated both anti-cancer and anti-angiogenic properties. Its anti-tumor properties include growth inhibition and apoptosis induction in a variety of cancer cell lines in vitro, as well as the ability to inhibit tumorigenesis in vivo.[1–7] Curcumin's anti-angiogenesis effects include the inhibition of vascular endothelial cell (VEC) proliferation in vitro and capillary tube formation and growth in vivo.[8,9] Because of its anti-cancer and anti-angiogenic properties, low molecular weight and lack of toxicity, curcumin could be an ideal candidate for a chemotherapeutic agent.[10] However, studies have demonstrated that its use is limited in vivo due to low potency and poor absorption characteristics.[11] This notwithstanding, curcumin remains a good lead compound for the design of analogs with a similar safety profile, but increased activity and solubility.

Biologic analyses of various curcumin derivatives have been conducted.[5,8,12,13] These studies focused mainly on changes in the β-diketone structure and aryl substitution pattern of the molecule. Our intent was to explore mono-carbonyl derivatives, diarylpentanoids, to see if they possess increased anti-cancer and anti-angiogenic activity and to pursue the mechanism of action of these derivatives. Before the compounds were synthesized, database searches were performed to identify commercially available mono-ketone analogs with potential for biological activity. A Unity/Tripos 2D similarity search of the Available Chemicals Database (ACD) produced two compounds with high similarity to curcumin: the mono-ketones 1,5-bis(3,4-dimethoxyphenyl)-1,4-pentadiene-3-one (BDMPP), **2**, and 2,6-bis((3-methoxy-4-hydroxyphenyl)-methylene)-cyclohexanone (BMHPC), **3** (Chart 1). BMHPC has been demonstrated to bind to nuclear type II sites on breast cancer cells with high affinity (K_d 1–7 nM) and to inhibit cell proliferation.[14] In the same study, a close relative of BMHPC, 2,6-bis((3,4-dihydroxyphenyl)-methylene)-cyclohexanone (BDHPC) was shown to inhibit mouse mammary tumor growth in vivo.[14] Both curcumin and its analogs have been shown to induce quinone reduction, quench superoxide radicals and stimulate Phase 2 enzyme transcription.[15] We tested **2** and **3** in a number of in vitro cell viability screens, and found the compounds to be more active than curcumin. As a follow-up, a number of novel mono-ketone lead compounds were synthesized and biologically evaluated as potential anti-cancer and anti-angiogenesis agent(s). In addition, compounds similar to those described herein have been probed recently as integrase inhibitors[16] and blockers of herpes simplex virus-1.[17] During the course of our work, a series of informative reports from the Dimmock–De Clercq team[18–21] and from El-Subbagh et al.[17] examined the broad-spectrum cell cytotoxicity of mono-ketones closely related to those under study here. As illuminated below, an important distinction between the latter studies and our own is the location of the aryl substitutents in the *ortho*-position. This and the utilization of an *ortho*-F instead of hydroxy or alkoxy substitutents appears to impart an unexpected boost in cell-kill activity. Accordingly, the main objective of the present investigation is the synthesis and testing of a number of symmetrical, but truncated curcumin analogs in order to develop novel, active and selective anti-cancer and anti-angiogenesis agent(s). In this paper, we describe the synthesis of curcumin analogs, which were tested in in vitro anti-cancer activity by us and the NCI. Furthermore, the best compound **14** was tested for in vivo antitumor effect.

2. Results and discussion

2.1. Chemistry

The target compounds depicted in Scheme 1 were obtained by allowing ketones to react with a variety of aromatic aldehydes under basic aldol condensation conditions to give the α,β-unsaturated ketones **4**–**8** and **10**–**13** (Table 1). Starting materials were selected to allow an assessment of the biological consequences of varying the substituents on the aromatic ring and the α-carbons of the ketone. All three mono-hydroxy

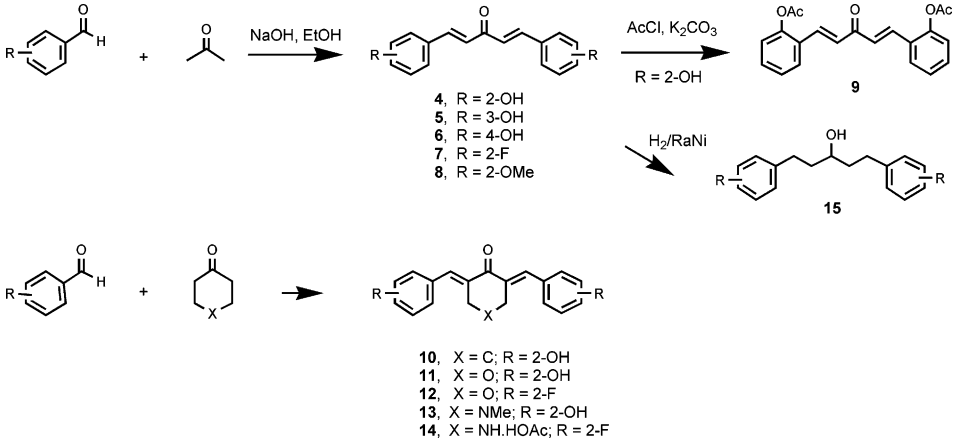

Scheme 1.

Table 1. Physical properties of synthesized curcumin analogs

No	Mp °C (solv)[a]	Formula	C, H, N calculated	C, H, N found
4	155 (A)	$C_{17}H_{12}O_3$	C, 76.68; H, 5.30	C, 76.56; H, 5.32
5	198–200 (A)	$C_{17}H_{12}O_3$	C, 76.68; H, 5.30	C, 76.41; H, 5.48
6	244–246 (A)	$C_{17}H_{12}O_3$	C, 76.68; H, 5.30	C, 76.48; H, 5.01
7	68–70 (B)	$C_{17}H_{12}F_2O$	C, 75.55; H, 4.48	C, 75.30; H, 4.55
8	122–123 (C)	$C_{19}H_{18}O_3$	C, 77.53; H, 6.16	C, 77.26; H, 6.17
9	128–130 (C)	$C_{21}H_{18}O_5$	C, 71.99; H, 5.18	C, 71.95; H, 5.46
10	148–149 (A)	$C_{20}H_{18}O_3$	C, 78.41; H, 5.92	C, 78.15; H, 6.03
11	148–150 (A)	$C_{19}H_{16}O_4$	C, 74.01; H, 5.23	C, 73.23; H, 5.23
12	157–158 (B)	$C_{19}H_{14}F_2O_2$	C, 73.07; H, 4.52	C, 73.07; H, 4.47
13	168–171 (D)	$C_{20}H_{17}NO_2$	C, 74.75; H, 5.96; N, 4.36	C, 75.11; H, 5.75; N, 4.68
14	186–189 (C)	$C_{21}H_{19}F_2NO_3$	C, 67.92; H, 5.16; N, 3.77	C, 68.63; H, 5.81; N, 3.52
15	68–70 (C)	$C_{17}H_{20}O_3$	C, 74.97; H, 7.40	C, 75.13; H, 7.44

[a] Solvents: A, acetone–H_2O; B, EtOAc–hexanes; C, EtOH; D, MeOH–H_2O.

substitution patterns on the aromatic rings were explored because of the reported increase in anti-carcinogenic activity for *ortho*-hydroxy groups.[12] In the present work, since *ortho*-substituents consistently exhibit better activity than their *meta* and *para*-counterparts (vide infra), we also explored replacement of the hydroxy groups with methoxy groups or fluorine. Annulation of the α-carbons allowed us to examine the preferred steric environment for this region of the structure, as well as to study the bio-effects of modifying hydrophilicity.

In the series of hydroxy-substituted benzaldehydes (**4**–**6**, **10**, **11**, **13**), chalcone derivatives **4**,[22,23] **6**,[16,24–26] and **10**,[13,27] were previously reported. The aldol condensations proceeded using an excess of base in aqueous ethanol. Yields of isolated products decreased significantly when the hydroxy group was moved from the *ortho*- to the *meta*- or *para*-positions (**4**, **5**, **6**). Prolonged reaction times (up to two weeks) or gentle warming did not positively affect the outcome of the reactions. By contrast, aldol reactions involving salicylaldehyde were considerably cleaner, producing **4** (75%), **10** (70%), **11** (60%), and **13** (75%) without complication. When fluoro- and methoxy-substituted aromatic aldehydes were allowed to react with ketones in the presence of base (NaOH), compounds **7**, **8**,[28] and **12** were obtained in analytically pure form and in moderate to good yields. Analog **14** was obtained using an acid promoted aldol condensation (glacial acetic acid), following the procedure described by McElvain and McMahon.[29] In addition, analogs **4** and **7**, both of which contain *ortho*-substituents on the aromatic rings, were either acetylated or reduced to the resulting derivatives, **9** and **15**.

2.2. Anticancer cell line screening

Curcumin analogs **10**, **11**, and **14** were subjected to the NCI's in vitro anti-cancer cell line screen, while the entire series **1**–**15** was examined in a variety of in vitro screens at Emory. In the NCI screen, 60 human tumor cell lines were treated for 48 h with 10-fold dilutions of compounds at a minimum of five concentrations (0.01–100 μM). A sulforhodamine B (SRB) endpoint assay was used to calculate three response parameters: median growth inhibition (GI_{50}), total growth inhibition (TGI), and median lethal concentration (LC_{50}).[30,31] GI_{50} refers to the concentration at which the drug inhibits tumor cell growth by 50%. TGI is defined as the concentration at which the drug inhibits tumor cell growth by 100%. LC_{50} is the concentration at which the drug decreases the original tumor cell number by 50% (50% tumor cell death). The NCI anti-cancer drug screen was designed to distinguish between compounds that have a broad spectrum of activity and those that are tumor or subpanel selective.[32] In the assays performed at Emory, human breast cancer (MDA-MB-231) and melanoma (RPMI-7951) cell lines were treated for 72 h with at least four different concentrations of compounds ranging from 0.1 to 50 μM. A Neutral Red cell viability assay[33] was used to determine a GI_{50} value for each compound (Table 4).

In the NCI anti-cancer cell line screen, the tested analogs showed a broad spectrum of activity, as well as distinctive patterns of selectivity. With regard to the broad-spectrum activity, Table 2 demonstrates that compounds **10**, **11**, and **14** are effective against all of the cell lines, as shown by their full panel mean-graph midpoint (MG-MID) values. The MG-MID is the calculated mean full panel or individual subpanel GI_{50}, TGI, or LC_{50}. The former MG-MID (μM) values are

Table 2. Full panel mean-graph midpoint (MG-MID) GI_{50}, TGI, LC_{50} values (μM)[a] of compounds in the NCI in vitro anti-cancer cell line screen[b]

	Full panel MG-MID		
Compounds	GI_{50}	TGI	LC_{50}
10	2.3	7.3	37.0
11	1.2	4.7	25.2
14	0.7	2.4	16.0
Cisplatin[c]	9.5	55.8	90.6
Curcumin[c]	7.3	23.5	67.2

[a] Calculated mean panel GI_{50}, TGI, or LC_{50}, which includes values at either limit (> or <).

[b] Human cancer cell lines were treated for 48 h with 10-fold dilutions of compounds at a minimum of five concentrations (0.01–100 μM). Sulforhodamine B (SRB) assay was used to calculate GI_{50}, TGI, or LC_{50} values. Data represents the mean of at least three experiments (except for compound **10**, $n = 1$).

[c] The values for cisplatin and curcumin are based on previous screens conducted by the NCI where the highest concentration tested was also 100 μM.

less than those for both curcumin and cisplatin when tested in the same manner. For example, the full panel MG-MID (μM) GI_{50} value for **14** (0.7) is 13.6- and 10.4-fold better than cisplatin (9.5) and curcumin (7.3), respectively. Table 2 also shows a TGI value for **14** (2.4) that is 23.3- and 9.8-fold more efficacious than cisplatin (55.8) and curcumin (23.5), respectively. Finally, this table illustrates that the LC_{50} value for **14** (16.0) is 5.7- and 4.2-fold improved over cisplatin (90.6) and curcumin (67.2), respectively. Cisplatin is a DNA cross-linking agent that is commonly used in the treatment of a number of different cancers, including testis, ovary, bladder, head and neck, and lung. While the exact target(s) of our compounds is not well understood, it is likely that the hydrophobicity and flexible molecular shapes of these agents allow them to enter the nuclear compartment where interaction with DNA (e.g., minor groove binding or strand cross-linking) could possibly occur. COMPARE analysis (see below) supports this hypothesis. Although compound **14** seems to be more effective than cisplatin in vitro, a direct comparison between these two agents against human tumor xenografts in nude mice could yield useful information as to compound **14**'s potential as an anti-cancer agent. The ratio obtained by dividing a compound's full panel MG-MID concentration by its individual subpanel MG-MID is considered as a measure of selectivity.[32] Ratios greater than 6 indicate high selectivity toward the corresponding cell line subpanel, while ratios between 3 and 6 refer to moderate selectivity. Compounds **11** and **14** both showed moderate selectivity toward leukemia cell lines based on GI_{50} values (Table 3).

Both Figure 1 and Table 3 demonstrate that compound **14** was similar to, but more active than both curcumin and cisplatin against each of the individual cancer subtypes. This drug was especially effective against leukemia, colon, CNS, prostate, and breast cancer cells with GI_{50} values less than 1.0 μM. Furthermore, Figure 1 shows that compound **14** was at least 10-fold more active than either curcumin or cisplatin against these cancer types. Table 3 demonstrates that analog **11** was effective against leukemia and prostate cancer cells (GI_{50} values less than 1.0 μM). Derivative **10** did not show GI_{50} values less than 1.0 μM for any tumor cell type, but did show effectiveness against individual cell lines such as leukemia RPMI-8226 and renal RXF-393 with GI_{50} values of 0.6 and 0.5 μM, respectively (data not shown).

Studies carried out at Emory focused on two highly malignant human cancer cell lines, RPMI 7951 (melanoma) and MDA-MB-231 (breast). The MDA-MB-231 cell line was also tested as part of the NCI screen, but the RPMI 7951 cell line was not. The GI_{50} values for **11** and **14** calculated against the breast cancer cell line were very similar to those calculated by the NCI. Both

Table 3. Mean growth inhibitory concentration (GI_{50}, μM)[a] of compounds in the NCI in vitro anti-cancer cell line screen[b]

	Cancer cell subpanel								
Compounds	Leukemia	NSCL[e]	Colon	CNS	Melanoma	Ovarian	Renal	Prostate	Breast
10	1.6 (1.4)[c]	3.1	2.1	2.5	2.2	3.3	2.0	1.7	2.5
11	0.4 (3.0)[c]	1.6	1.1	1.4	1.5	1.4	1.3	0.8	1.6
14	0.2 (3.5)[c]	1.1	0.3	0.5	1.4	0.8	0.7	0.4	0.6
Cisplatin[d]	6.3	9.4	21.0	4.7	8.5	6.3	10.2	5.6	13.3
Curcumin[d]	3.7	9.2	4.7	5.8	7.1	8.9	8.9	11.2	5.9

[a] 50% Growth inhibition (micro-molar concentration of compounds, which causes a 50% inhibition of cell growth).
[b] See footnote b from Table 2.
[c] GI_{50} selectivity ratios obtained by dividing the compound's full panel GI_{50} MG-MID (μM) (Table 2) by its leukemia subpanel MG-MID are shown in parentheses. A selectivity ratio greater than 3.0 suggests that the compound is potentially more active against a particular type of cancer cell.[32]
[d] See footnote c from Table 2.
[e] Nonsmall cell lung cancer.

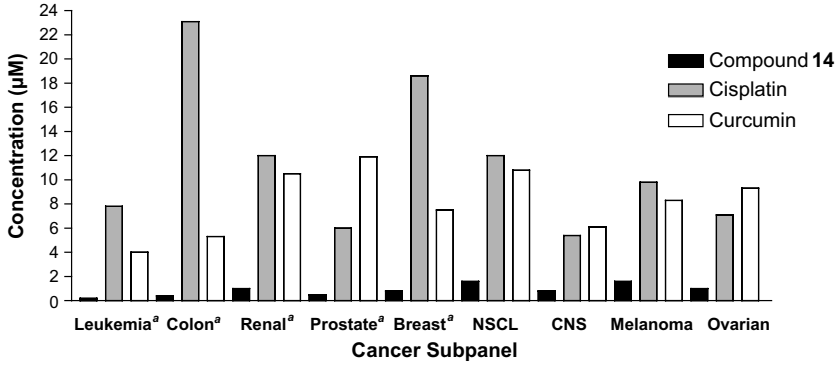

Figure 1. Mean growth inhibitory concentration (GI_{50}) of compound **14** compared to cisplatin and curcumin in a subset of cells in the NCI in vitro anti-cancer screen. Compound **14** is more active than both of the latter agents against a wide variety of cancer types[a] and at least 10-fold more potent than either curcumin or cisplatin against the nine cancer types presented.

Table 4. Mean growth inhibitory concentration (GI_{50}, μM)[a] of compounds in the Emory University in vitro anti-cancer cell line screen[b]

	Cancer cell line	
Compounds	Melanoma RPMI 7951	Breast MDA-MB-231
Curcumin (**1**)	4.5 ± 2.1	11.1 ± 1.1
BDMPP (**2**)	3.3 ± 2.5	5.4 ± 0.8
BMHPC (**3**)	3.4 ± 2.2	5.0 ± 0.0
4	1.0 ± 0.5	2.3 ± 0.5
5	2.8 ± 0.2	3.9 ± 0.2
6	5.7 ± 0.9	7.5 ± 0.7
7	8.5 ± 0.3	12.6 ± 0.5
8	1.8 ± 0.5	3.1 ± 0.5
9	1.9 ± 1.5	2.7 ± 0.7
10	3.0 ± 0.9	3.6 ± 0.0
11	0.8 ± 0.0	0.8 ± 0.0
12	1.9 ± 0.0	6.5 ± 0.0
13	0.9 ± 0.0	1.9 ± 0.1
14	0.7 ± 0.0	0.8 ± 0.4

[a] See footnote a from Table 3.

[b] Human melanoma and breast cancer cell lines were treated for 72 h with at least four different concentrations of compounds ranging from 0.1 to 50 μM. Neutral Red cell viability assay[33] was used to calculate a GI_{50} value for each compound. Data represents the mean ± SD of 2–5 experiments performed in duplicate.

compounds produced a value of 0.8 μM in our study (Table 4), while **14** produced a value of 1.0 μM and **11** produced a value of 1.1 μM in the NCI study (data not shown). The two compounds were the most effective against both cell lines tested in this study, in agreement with the results of the NCI screen.

Among the bis-benzylidene-acetone analogs (**4**–**9**), compound **4** showed the highest activity based on GI_{50} (Table 4). The presence of *ortho*-OH was previously shown to be important for activity in other curcumin analogs.[12] This effect is confirmed by our assays. Analyzing the data for the hydroxy-substituted derivatives (**4**–**6**) revealed that moving the OH from the *ortho*- to the *para*-position (as in curcumin) decreased cytotoxicity (**4** > **5** > **6**). Replacing the hydroxyl group in **4** with methoxy, **8**, or fluorine, **7**, led to a slight decrease in activity. Also, esterifying **4** to compound **9** decreased activity only very slightly, implying that under the assay conditions the esters are probably hydrolyzed. Among the unsaturated analogs derived from cyclic ketones (**10**, **11**, **12**, **13**, **14**), all of the analogs with *ortho*-hydroxyl groups (**10**, **11**, and **13**) exhibited good activity. The introduction of heteroatoms in the six-membered ring (tetrahydropyran and piperidine) produced derivatives **11** and **13** that were more active than compound **4**. The oxygen-analog (**11**) was slightly more active than the *N*-methyl-piperidone derivative **13**. The *ortho* fluoro-substituted piperidone analog **14** was the most active compound in the NCI screen and in the assays performed at Emory. The arylethyl alcohol **15** was devoid of any cytotoxic activity at concentrations up to 50 μM (data not shown).

2.3. Anti-angiogenesis screening

Curcumin analogs **10**, **11**, and **14** were subjected to the NCI's in vitro anti-angiogenesis screen. In addition, all analogs were subjected to in vitro proliferation assays at Emory. The NCI analysis consists of three assays, growth inhibition, cord formation, and cell migration. Only the results of the cord formation and cell migration assays are presented (Table 5) since growth inhibition was studied at Emory (Table 6). In the cord formation assay, HUVECs were allowed to form cords on matrigel-coated plates. Drug effect after 24 h compared to untreated controls was assessed by measuring the length of cords formed and the number of junctions. The cell migration assay was conducted using a Boyden chamber system and collagen-coated polycarbonate filters. The ability of the drugs to inhibit HUVEC migration toward a chemo-attractive source (bFGF, VEGF, or Swiss 3T3 conditioned medium) was determined by examining the number of cells that migrated onto the filter. Negative, unstimulated control values were subtracted from stimulated control and drug treated values, and the data was plotted as mean migrated cell ± SD. The IC_{50} was

Table 5. Mean inhibitory concentration (IC_{50}, μM)[a] of compounds in the NCI in vitro anti-angiogenesis screen[b]

	Assay	
Compound	Cord formation	Cell migration
Curcumin (**1**)	>10	1.8 ± 0.1
10	>30	5.0 + 0.0
11	6.5 ± 0.7	7.1 ± 0.1
14[c]	1.5 ± 0.4	0.8 ± 0.1
TNP-470	0.7 ± 0.2	0.6 ± 0.0

[a] 50% Inhibitory concentration (molar concentration of compounds, which causes a 50% inhibition as compared to control).

[b] Human Umbilical Vein Endothelial Cells (HUVECs) were used to examine the effects of the compounds on cord formation and cell migration. Data represents the mean of at least two experiments performed in replicates of 2–8.

[c] Compound **14** was equipotent to TNP-470 in the Cord Formation assay and only 2-fold less potent in the cell migration assay.

Table 6. Mean growth inhibitory concentration (GI_{50}, μM)[a] of compounds in the Emory University in vitro anti-angiogenesis screen[b]

	Cell line		
Compounds	HUVEC	MS1	SVR
Curcumin (**1**)	16.6 ± 5.6	5.9 ± 1.6	9.8 ± 2.0
BDMPP (**2**)	3.6 ± 1.4	1.9 ± 1.5	3.3 ± 2.9
BMHPC (**3**)	12.0 ± 3.8	4.4 ± 2.2	5.4 ± 3.2
4	1.8 ± 1.2	1.8 ± 1.4	2.2 ± 1.4
5	3.2 ± 0.3	4.1 ± 1.6	4.4 ± 0.6
6	7.6 ± 2.4	6.0 ± 1.1	5.5 ± 1.4
7	6.1 ± 2.9	9.0 ± 2.4	10.3 ± 0.2
8	6.8 ± 1.9	1.6 ± 1.0	3.1 ± 0.9
9	2.3 ± 1.4	1.1 ± 0.9	2.9 ± 2.9
10	8.0 ± 4.5	2.0 ± 2.1	3.5 ± 2.3
11	2.9 ± 3.4	0.8 ± 0.3	1.5 ± 1.6
12	4.1 ± 0.7	8.0 ± 0.7	8.5 ± 1.6
13	4.0 ± 2.2	2.1 ± 0.1	1.6 ± 0.6
14	1.1 ± 0.5	1.1 ± 0.2	1.2 ± 0.5

[a] See footnote a from Table 3.

[b] Human and murine endothelial cell lines were treated for 72 h with compounds at a minimum of four concentrations between 0.1 and 50 μM. Neutral Red assay[33] was used to calculate a GI_{50} value for each compound. Data represents the mean ± SD of 2–7 experiments performed in duplicate.

calculated from the plotted data. The Emory anti-angiogenesis screen focused on the ability of the compounds to inhibit endothelial cell growth in vitro. HUVECs, and two SV40 large T antigen-immortalized murine endothelial cell lines, MS1 and SVR[34], were treated for 72 h with at least four different concentrations of compounds ranging from 0.1 to 50 μM (Table 6). The SVR cells also contain a mutant *H-ras* gene. A Neutral Red cell viability assay[33] was used to calculate the GI_{50} value for each compound.

The NCI data demonstrated that compounds **10**, **11**, and **14** were effective against angiogenesis in both of the assays described above (Table 5). Compound **14** was almost as potent as the anti-angiogenesis drug, TNP-470, in the cell migration assay, with IC_{50} values of 0.6 μM (TNP-470) and 0.8 μM (**14**). TNP-470 was slightly more potent than **14** in the cord formation assay, with IC_{50} values of 0.7 μM (TNP-470) and 1.5 μM (**14**). TNP-470 has proven to be effective in vitro and in animal model studies and is currently being tested in Phase III clinical trials.[35] Furthermore, compound **14** was more active than curcumin in both of the assays. This is seen especially in the cord formation assay where the IC_{50} values were >10 μM (curcumin) and 1.5 μM (**14**).

In the experiments performed at Emory, the same general pattern observed for the anti-cancer testing was also seen in the anti-angiogenesis screen (Table 6). Compound **4** showed the highest activity among the bis-benzylidene-acetone analogs (**4**, **5**, **6**, **7**, **8**). In line with the observations mentioned above, moving the OH from the *ortho*- to *para*-position in the hydroxy-substituted derivatives (**4**, **5**, **6**) decreases cytotoxicity (**4** > **5** > **6**). Furthermore, replacement of the hydroxyl group in **4** with a methoxy (as in **8**) or a fluorine group (as in **7**) leads to a slight decrease in activity. The unsaturated analogs derived from cyclic ketones that contain *ortho*-hydroxyl groups (**10**, **11**, and **13**) demonstrated good activity, while the introduction of heteroatoms into carbocyclic ketones (cf., tetrahydropyran derivative **11**) leads to compounds that are slightly more active than **4**. As was seen in the anti-cancer screen, the oxygen-analog (**11**) is slightly more active than the *N*-methyl-piperidone derivative (**13**). The *ortho*-fluoro substituted analog **14** was the most active compound in the NCI anti-angiogenesis screen and in the Emory assay. Again, the arylethyl alcohol (**15**) lacked any anti-angiogenic activity (data not shown).

2.4. In vivo antitumor activity and toxicity

Since compound **14** proved to be the most active compound in the in vitro anti-cancer and anti-angiogenesis screens, further tests were performed to measure the activity of this compound in vivo. The ability of compound **14** to induce tumor regression was examined by growing solid breast tumors in the flanks of female athymic nude (nu/nu) mice. After three weeks of tumor growth, drug was administered subcutaneously near the base of the tumor for two weeks. Figure 2 shows a dose dependent decrease in tumor weight after

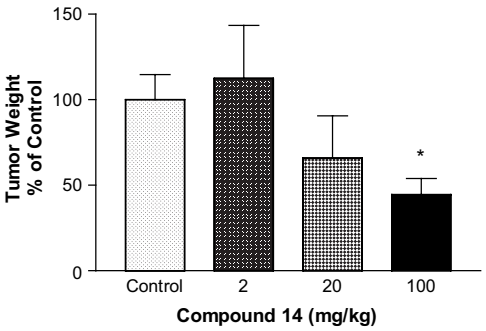

Figure 2. Regression of breast tumors in nude mice after treatment with compound **14**. 1,000,000 MDA-MB-231 breast cancer cells were inoculated in the flanks of nude mice and tumors were allowed to grow for three weeks. Compound **14** was administered by injection near the base of the tumors three times a week for two weeks. The graph demonstrates a dose dependent decrease in tumor weight after treatment ($^{*}p < 0.05$; $n = 5$ mice/group).

treatment with compound **14**. While there was no difference between the average tumor weight of the 2 mg/kg group and control group, the average tumor weight in the 20 mg/kg group was decreased to about 70% of the control value, and that of the 100 mg/kg group decreased to about 45%. Although the latter dose appears to be slightly above the practical treatment range, it was necessary to effectively treat the extremely large tumors. Remarkably, the 100 mg/kg dose demonstrated no harmful side effects. No liver, kidney, or spleen toxicity was seen, and all of the treated mice demonstrated normal weight gain (data not shown). Furthermore, this dose was well below the maximum tolerated dose (MTD) of 200 mg/kg iv (400 mg/kg ip) determined by the NCI. The MTD is calculated as the dose above which the animals die from a single bolus injection. Compound **14** appears to be much safer than Cisplatin, which shows an MTD of 10 mg/kg ip. Thus, **14** seems to have potential as a chemotherapeutic agent since it demonstrates better activity but lower toxicity than a commonly used drug.

2.5. Structure–activity correlation

In a first attempt to develop a quantitative structure activity correlation, we have employed the quasi-atomistic receptor model embedded in Quasar 3.5.[36] The method requires a chemically meaningful superposition of ligands accompanied by realistic atomic charges and a reliable set of biological responses. The ligands are divided into training and test sets. Subsequently, a genetic algorithm is employed to iteratively construct a three-dimensional envelope of complementary atomistic probes about each ligand in the training set until such envelopes provide the best 'prediction' of the biological data. In the present instance, the similarity of structures presented no difficulty in the development of a suitable molecular alignment (see Experimental). The responses of the breast cancer cell line MDA-MB-231 to the curcuminoids (Table 4) were taken as a representative sample of the biological data. Nineteen compounds

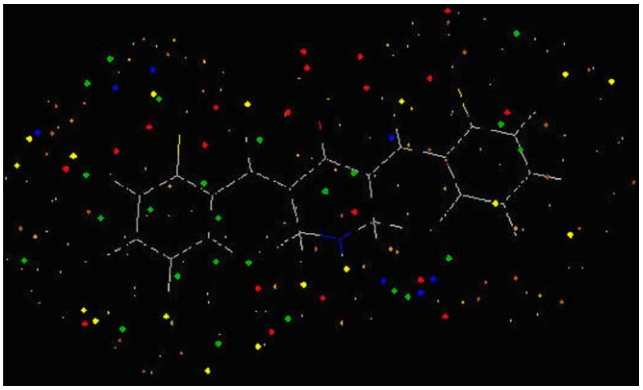

Figure 3. Average quasi-atomistic receptor model (Quasar 3.5) for the curcuminoids derived by using compound **14** (pictured) as the pharmacophore template. The Quasar receptor probes are colored as follows: positively-charged salt bridge (red), negatively-charged salt bridge (blue), H-bond donor (green), H-bond acceptor (yellow), positively charged hydrophobic (saddle brown), negatively charged hydrophobic (chocolate brown), H-bond flip-flop (purple), solvent (cyan).

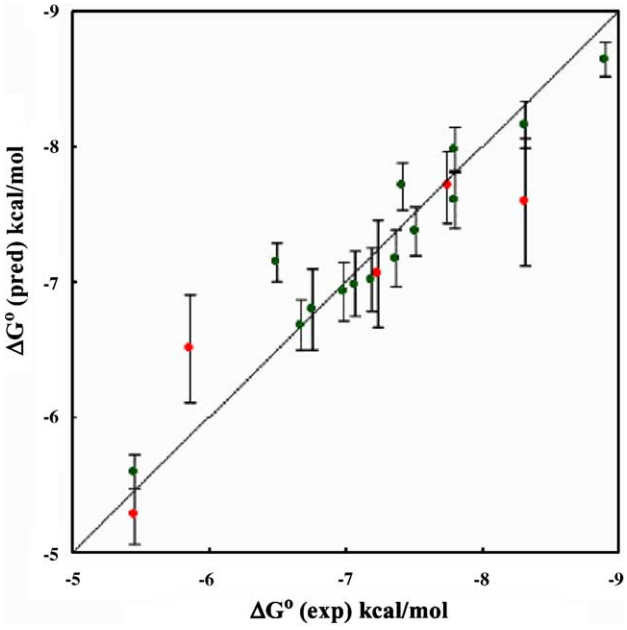

Figure 4. Quasar correlation of the curcuminoid quasi-atomistic model shown in Figure 3; r^2 0.85, cross-validated $r^2(q^2)$ 0.83, predictive $r^2(p^2)$ 0.71; training set, green; test set, red. For error bars, see Experimental.

with GI_{50}'s ranging from 0.8 to 100 μM were assembled.[37] The same structures were encoded as a total of 114 conformers. For convenience in processing by Quasar, the GI_{50}'s were expressed as ΔG's (kcal/mol). For the training set, the resulting correlation gave an $r^2 = 0.85$, a cross-validated $r^2(q^2) = 0.83$, an rms deviation of 0.24 kcal/mol and a maximum deviation of 0.64 kcal/mol. Similar statistics arise for the test set (see Experimental). Figure 3 displays the average quasi-atomistic receptor model for the entire class of curcuminoids surrounding the highly active prototype **14**. While there is a fair amount of scatter in the probe types from the model averaging process (see Experimental), the central carbonyl is appropriately surrounded by a cluster of red probes corresponding to a positively charged salt-bridge. Likewise, the piperidone nitrogen is associated with a yellow probe, namely a hydrogen-bond acceptor.

Figure 4 depicts the overall correlation of training and test sets, which represent GI_{50}'s in terms of ΔG° over a 3.5 kcal/mol range. Scramble tests applied to the data demonstrate the correlation to be robust (see Experimental). Active and inactive compounds can be distinguished quite clearly. The substantial predictive $r^2(p^2) = 0.71$ provides a useful tool for future synthetic planning.

Efforts to relate structural modifications of the mono keto-curcumin analogs with the observed anti-cancer and anti-angiogenesis data support the following general conclusions:

(1) The symmetrical α,β-unsaturated ketone structure found in the novel analogs shows increased in vitro anti-cancer and anti-angiogenesis activity compared to the β-diketone structure of curcumin.
(2) *ortho*-Substitution on the aromatic rings (as for **4**, **10**, **11**, **13**, **14**) enhances the activity of the symmetrical analogs. Compounds with substitutions in the *meta*- or *para*-positions (**5** and **6**) are not as active.
(3) The introduction of heteroatoms in the cyclic ketone portion (**11**, **12**, **13**, **14**) yields compounds with improved anti-cancer and anti-angiogenesis activity.
(4) Saturation of the olefinic bond of one of the α,β-unsaturated ketones produced an arylethyl alcohol (**15**) that possessed little anti-cancer and direct anti-angiogenic activity. While the unsaturated compounds are likely acting as Michael acceptors, which would normally result in unacceptable toxicity levels, the high MTD suggests that the Michael additions may be occurring selectively in tumor cells. Consistent with this hypothesis, treatment of tumor-bearing mice with compound **14** represses the tumors but shows no evidence of toxicity in the animals.

2.6. Possible mechanisms of action; COMPARE

In order to gain insight into the possible biological basis for the cytotoxic action of compound **14**, we performed a COMPARE analysis[48] against compounds exposed to the NCI's 60-cell line assay panel. Three indicators are provided by the database: GI_{50} (growth inhibition), LC_{50} (lethal concentration), and TGI (total growth inhibition). Averaging over the top 25 hits in each category, the dominant suggested mechanism is an RNA/DNA antimetabolite (36% of total). This was followed by topoisomerase II inhibition and antimitotic action, each of which registered at 8%. Interestingly, the largest category for the compound was 'unknown' (40%). Consequently, the cytotoxic behavior of **14** may represent a new mechanism for controlling tumor cell proliferation. This question is under active investigation.

3. Conclusions

The synthetic curcumin analogs prepared in this study were effective in anti-cancer and anti-angiogenesis screens performed both at Emory University and at the NCI. The compounds were more efficacious than curcumin and the commonly used chemotherapeutic drug, cisplatin against a variety of tumor cell lines. In the NCI anti-cancer screen, **10**, **11**, and **14** all show remarkable cytotoxic activity, while **11** and **14** demonstrate selectivity toward leukemia cell lines. The studies also demonstrate the compounds to exert impressive blockade of endothelial cell proliferation. In the NCI anti-angiogenesis assays, **10**, **11**, and **14** were potent inhibitors of cord formation and cell migration, and compound **14** was just as potent as TNP-470 in both of these assays. **14** also effectively induced regression of large human breast tumors in mice and demonstrated little toxicity during the treatment. Finally, it is important to mention that this compound has been selected by the NCI for further evaluation. Depending upon the results of these and other studies, compound **14** may represent a promising lead for clinical development. In the search for backup compounds, we expect that the 3D-QSAR based on **14** will provide insights and synthetic guidance.

4. Experimental

All reagents were obtained from commercial suppliers and used without further purification. Reaction progress was monitored through thin layer chromatography (TLC) on pre-coated glass plates (silica gel 60 F^{254}, 0.25 mm thickness) purchased from EM Science. Flash chromatography was carried out with silica gel 60 (230–400 mesh ASTM) from EM Science. ^{1}H NMR and ^{13}C NMR spectra were recorded on a Mercury 300 or Varian 400 spectrometer. Unless otherwise specified, all NMR spectra were obtained in deuterated chloroform ($CDCl_3$) and referenced to the residual solvent peak; chemical shifts are reported in parts per million, and coupling constants in hertz (Hz). Melting points were determined on a Thomas Hoover capillary melting point apparatus and are uncorrected. Mass spectra were obtained on either a VG 70-S Nier Johnson or JEOL Mass Spectrometer. Elemental analyses were performed by Atlantic Microlab (Norcross, GA) for C, H, and N and agreed with the proposed structures within ±0.4% of the theoretical values. The syntheses of compounds **4**,[15,16] **6**,[16–19] **8**,[23] **9**,[38] and **10**[13,20] have been previously reported.

4.1. General procedure for preparation of hydroxy-substituted 3,5-bis-(arylidene)-ketones 4, 5, 6, 10, 11, and 13

Aqueous NaOH (20 wt %, 15 mL, 75 mmol) was added dropwise to a vigorously stirred solution of the appropriate hydroxy-benzaldehyde (51 mmol) and ketone (25 mmol) in abs EtOH (20 mL). The reaction was stirred at room temperature (RT) for 48 h, then 100 mL distd H_2O added, and the resulting purple solution was neutralized by gently bubbling CO_2 through it. The yellow precipitate was filtered off, washed with distd H_2O, and dried under vacuum. The products were purified by recrystallization from the indicated solvent(s).

4.1.1. 1,5-Bis-(2-hydroxyphenyl)-penta-1,4-dien-3-one (4). The crude product was recrystallized from acetone/H_2O to give **4** as a yellow solid (75%): mp 155 °C [lit.[15] 159 °C (EtOH)]. ^{1}H NMR (400 MHz, CD_3OD) δ 8.09 (d, $J = 16$ Hz, 2H), 7.63 (dd, $J = 8.4$, 1.6 Hz, 2H), 7.31 (d, $J = 16$ Hz, 2H), 7.24 (td, $J = 7.6$, 1.6 Hz, 2H), 6.88 (t, $J = 7.2$ Hz, 4H). ^{13}C NMR (100 MHz, CD_3OD) 192.80, 158.90, 140.97, 133.10, 130.21, 126.33, 123.23, 121.00, 117.23. HREIMS: m/z 248.0845 ($(M-H_2O)^+$, $C_{17}H_{12}O_2$ requires 248.0837).

4.1.2. 1,5-Bis-(3-hydroxyphenyl)-penta-1,4-dien-3-one (5). The crude product was recrystallized from acetone/H_2O to produce **5** as a yellow solid (15%): mp 198–200 °C. ^{1}H NMR (400 MHz, CD_3OD) δ 7.70 (d, $J = 16$ Hz, 2H), 7.24 (t, $J = 7.6$ Hz, 2H), 7.17 (d, $J = 16$ Hz, 2H), 7.17 (d, $J = 8$ Hz, 2H), 7.11 (s, 2H), 6.73 (dd, $J = 8$, 2.4 Hz, 2H). ^{13}C NMR (100 MHz, CD_3OD) δ 191.61, 159.25, 145.47, 137.61, 131.20, 126.36, 121.41, 119.09, 115.88. HREIMS: m/z 266.0946 (M^+, $C_{17}H_{14}O_3$ requires 266.0943).

4.1.3. 1,5-Bis-(4-hydroxyphenyl)-penta-1,4-dien-3-one (6). The crude product was recrystallized from acetone/H_2O to produce **6** as a yellow solid (6%): mp 244–246 °C [lit.[17] 248–250 °C]. ^{1}H NMR (400 MHz, CD_3OD) δ 7.71 (2H, d, $J = 16$ Hz), 7.58 (4H, d, $J = 8.8$ Hz), 7.07 (2H, d, $J = 16$ Hz), 6.84 (4H, d, $J = 8.4$ Hz). ^{13}C NMR (100 MHz, CD_3OD) δ 191.86, 161.79, 145.34, 131.84, 127.84, 123.57, 117.07. HREIMS: m/z 266.0948 (M^+, $C_{17}H_{14}O_3$ requires 266.0943).

4.1.4. 2,6-Bis-(2-hydroxybenzylidene)-cyclohexanone (10). The crude product was recrystallized from acetone/H_2O to produce **10** as a yellow solid (70%): mp 148–149 °C [lit.[21] 150 °C ($CHCl_3$)]. ^{1}H NMR (400 MHz, CD_3OD) δ 7.98 (2H, s,), 7.32 (2H, dd, $J = 7.6$, 1.2 Hz), 7.19 (2H, td, $J = 7.6$, 1.2 Hz), 6.86 (4H, m), 2.86 (4H, m), 1.75 (2H, m). ^{13}C (100 MHz, CD_3OD) δ 192.88, 158.18, 137.26, 134.48, 131.55, 124.45, 120.21, 116.62, 29.93, 24.78. HREIMS: m/z 306.1263 (M^+, $C_{20}H_{18}O_3$ requires 306.1256).

4.1.5. 3,5-Bis-(2-hydroxybenzylidene)-tetrahydro-4-*H*-pyran-4-one (11). The crude product was recrystallized from acetone/H_2O to yield **11** as a yellow solid (60%): mp 148–150 °C. ^{1}H NMR (400 MHz, CD_3OD) δ 8.08 (2H, s), 7.24 (2H, td, $J = 8.4$, 1.6 Hz), 7.09 (2H, dd,

$J = 7.6, 1.6$ Hz), 7.90–7.86 (4H, m), 4.84 (4H, d, $J = 1.6$ Hz). ^{13}C NMR (100 MHz, CD_3OD) δ 187.82, 158.48, 133.93, 132.46, 131.88, 123.29, 120.47, 116.80, 70.02. HREIMS: m/z 290.0933 (M^+, $C_{19}H_{16}O_4$ requires 290.0943).

4.1.6. 3,5-Bis-(2-hydroxybenzylidene)-1-methyl-4-piperidone (13). The crude product was recrystallized from methanol/H_2O to produce **13** as a yellow solid (75%): mp 168–171 °C. ^{1}H NMR (400 MHz, CD_3OD) δ 8.11 (2H, s), 7.23 (4H, t, $J = 7.6$ Hz), 6.88 (4H, t, $J = 8.0$ Hz), 3.76 (4H, d, $J = 1.2$ Hz), 2.42 (3H, s). ^{13}C NMR (100 MHz, CD_3OD) δ 188.40, 158.58, 135.09, 133.09, 132.27, 131.64, 123.59, 120.38, 116.87. HREIMS: m/z 303.1259 (M^+-H_2O, $C_{20}H_{17}NO_2$ requires 303.1259).

4.2. General procedure for preparation of fluoro-substituted 3,5-bis-(arylidene)-ketones 7 and 12

A solution of substituted fluorobenzaldehyde (5.00 mmol) in EtOH abs (1 mL) was added at room temperature over a period of 5 min, with stirring, to a solution of NaOH (0.75 mmol) and ketone (2.50 mmol) in a mixture of EtOH abs (7 mL) and H_2O distd (7 mL). The solution turns yellow immediately, and within 10 min, **7** produced a yellow oil, while **12** produced a yellow precipitate. Stirring was continued at room temperature for 3 h.

4.2.1. 1,5-Bis-(2-fluorophenyl)-penta-1,4-dien-3-one (7). The product was produced as a yellow oil and isolated from the reaction mixture after diluting with H_2O dist by extraction with CH_2Cl_2 (3×). The combined organic layers were dried over $MgSO_4$ and concentrated. The crude product was purified by column chromatography on silica gel (15% EtOAc/hexanes) yielding the product as a yellow solid (50%): mp 68–70 °C. ^{1}H NMR (400 MHz, $CDCl_3$,) δ 7.86 (2H, d, $J = 16$ Hz), 7.63 (2H, td, $J = 7.6, 1.6$ Hz), 7.42–7.35 (2H, m), 7.18 (2H, d, $J = 16$ Hz), 7.26–7.10 (4H, m). ^{13}C NMR (100 MHz, $CDCl_3$) δ 189.17, 161.84 (d, $J = 253$ Hz), 136.30 (d, $J = 2$ Hz), 132.13 (d, $J = 9$ Hz), 129.56 (d, $J = 2$ Hz), 127.78 (d, $J = 6$ Hz), 124.73 (d, $J = 4$ Hz), 123.03 (d, $J = 11$ Hz), 116.47 (d, $J = 22$ Hz). HREIMS: m/z 270.0865 (M^+, $C_{17}H_{12}F_2O$ requires 270.0856).

4.2.2. 3,5-Bis-(2-fluorobenzylidene)-tetrahydro-4-*H*-pyran-4-one (12). The obtained yellow solid, was filtered off, washed with water and hexanes, and dried under vacuum. The crude product was recrystallized from EtOH yielding **12** (84%): mp 157–158 °C. ^{1}H NMR (400 MHz, $CDCl_3$) δ 7.92 (2H, d, $J = 1.2$ Hz), 7.40–7.36 (2H, m), 7.20–7.18 (4H, m), 7.13 (2H, t, $J = 9.6$ Hz), 4.80 (4H, s). ^{13}C NMR (100 MHz, $CDCl_3$) δ 185.09, 161.04 (d, $J = 251$ Hz), 134.78, 131.54 (d, $J = 9$ Hz), 131.08 (d, $J = 2$ Hz), 129.56 (d, $J = 4$ Hz), 124.30 (d, $J = 4$ Hz), 122.84 (d, $J = 14$ Hz), 116.23 (d, $J = 22$ Hz), 68.91 (d, $J = 5$ Hz). HREIMS: m/z 312.0950 (M^+, $C_{19}H_{14}F_2O_2$ requires 312.0962).

4.3. 1,5-Bis-(2-methoxyphenyl)-penta-1,4-dien-3-one (8)

NaOH (0.10 mmol) was added as a solid to a stirred solution of 2-methoxybenzaldehyde (2.50 mmol) and acetone (1.20 mmol) in EtOH abs (5 mL). A yellow solid started forming within one hour, stirring was continued at room temperature for 20 h, the product filtered off, washed with cold EtOH abs and H_2O distd, and dried under vacuum yielding **8** as a yellow solid (60%): mp 122–123 °C (EtOH), [lit.[21,39,40] 120–121 °C (EtOH)]. ^{1}H NMR (400 MHz, $CDCl_3$) δ 8.07 (2H, d, $J = 16$ Hz), 7.63 (2H, dd, $J = 7.6, 1.6$ Hz), 7.37 (2H, ddd, $J = 7.2$ Hz, $J = 1.6$ Hz, $J = 1.2$ Hz), 7.18 (2H, d, $J = 16$ Hz), 6.99 (2H, t, $J = 7.6$ Hz), 6.93 (2H, d, $J = 8.4$ Hz). ^{13}C NMR (100 MHz, $CDCl_3$) δ 190.21, 158.74, 138.39, 131.78, 128.89, 126.42, 124.12, 120.92, 111.35, 55.70. HREIMS: m/z 294.1256 (M^+, $C_{19}H_{18}O_3$ requires 294.1256).

4.4. 1,5-Bis-(2-acetylphenyl)-penta-1,4-diene-3-one (9)

This was obtained by acetylation of **4** using acetylchloride (2.4 equiv) and K_2CO_3 (3 equiv) in THF. The crude product was recrystallized from EtOH and obtained as a yellow solid (80%): mp 128–130 °C, [lit.[38] 129 °C (EtOH)].

4.5. 3,5-Bis-(2-fluorobenzylidene)-piperidin-4-one, acetic acid salt (14)

4-Piperidone hydrochloride monohydrate (307 mg, 2.00 mmol) was suspended in glacial acetic acid (8 mL) and saturated with HCl gas at room temperature. To the resulting clear solution 2-fluorobenzaldehyde (0.59 mL, 5.60 mmol) was added and the reaction allowed to stand at room temperature for 48 h. The forming yellow crystals were filtered off, washed with EtOH abs, and dried under vacuum yielding **14** as yellow plates (91%): mp 186–189 °C. ^{1}H NMR (400 MHz, DMSO-d_6) δ 10.11 (1H, s-br), 7.90 (2H, s), 7.57 (2H, qd, $J = 7.6, 1.6$ Hz), 7.51 (2H, td, $J = 8.0, 1.2$ Hz), 7.37 (4H, q, $J = 10.0$ Hz), 4.37 (4H, s), 3.60–3.20 (1H, s-br), 1.91 (3H, s). ^{13}C NMR (100 MHz, DMSO-d_6) δ 181.95, 172.04, 160.33 (d, $J = 249$ Hz), 132.57 (d, $J = 9$ Hz), 131.81 (d, $J = 4$ Hz), 131.05, 129.86, 124.96 (d, $J = 3$ Hz), 121.49 (d, $J = 13$ Hz), 116.1 (d, $J = 21$ Hz), 43.79, 21.11. HREIMS: m/z 311.1123 (M^+–HOAc, $C_{19}H_{15}NOF_2$ requires 311.1122).

4.6. General procedure for preparation of substituted saturated alcohols 15

Alcohols **15** were obtained by hydrogenation of **4** or **7** in EtOH abs at 45 psi for 4 h using Raney Nickel as the

catalyst. Filtration through Celite and concentration under vacuum yielded the crude product, which was purified by chromatography on silica gel (25% EtOAc/hexanes). Reaction progress can be detected by disappearance of the yellow color of the starting materials. Excessive hydrogenation yielded alcohols (**15**) exclusively (white solids, 60–80% yield: R = 2-OH; mp 79–81 °C, R = 2-F; mp 68–70 °C (Scheme 1)).

4.7. Cell culture

RPMI-7951 human melanoma and MDA-MB-231 human breast cancer cells were purchased from American Type Cell Collection (ATCC), Rockville, MD. Human Umbilical Vein Endothelial Cells (HUVECs) were obtained from the Department of Dermatology, Emory University. Murine endothelial cells infected with either simian virus 40 (SV40) large T antigen (MS1) or SV40 large T antigen and activated H-ras (SVR) were a kind gift from Dr. Jack Arbiser at Emory. RPMI 7951 and MDA-MB-231 cell lines were maintained in MEM-alpha medium (GIBCO-BRL, Long Island, NY) containing 10% fetal bovine serum (FBS) (Mediatech, Herndon, VA), penicillin (100 units/mL) and streptomycin (100 μg/mL) and 2 mM L-glutamine. Cells were incubated at 37 °C in 5% CO_2, 95% air in a humid atmosphere. MS1 and SVR cell lines were cultured in DMEM (Mediatech, Herndon, VA) containing 10% fetal bovine serum (FBS) (Mediatech, Herndon, VA), penicillin (100 units/mL), streptomycin (100 μg/mL) and 2 mM L-glutamine. HUVECs were cultured in M199 medium (GIBCO-BRL) containing 20% FBS, penicillin (100 units/mL), streptomycin (100 μg/mL), amphotericin B as Fungizone (0.25 μg/mL), 2 mM L-glutamine, heparin (10,000 units/mL), and endothelial mitogen. In order to avoid mutational changes of cells lines, cells have been expanded in culture, aliquoted, and stored in a liquid nitrogen freezer when purchased from the ATCC.

4.8. Neutral red assay for cell viability

This assay was carried out according to the methods published by Zhang et al.[33] Tumor cells (MDA-MB-231, RPMI 7951) for the anti-cancer screen, or endothelial cells (HUVEC, MS1, SVR) for the anti-angiogenesis screen were plated at a concentration of 20,000 cells/well in a 48-well plate and incubated overnight. Compounds or vehicle, dimethyl sulfoxide (DMSO 0.1% (Sigma, St. Louis, MO)) were then added and the plates were incubated for 72 h. Supernatant from each well was aspirated and warm (37 °C) media containing Neutral Red (stock-3.33 μg/μL) solution (GIBCO-BRL, Long Island, NY) was added at a concentration of 50 μg/mL (approximately 15 μL/mL medium). The plates were incubated at 37 °C for 30 min. In principle, only viable cells take up the Neutral Red dye. Next, the cells were washed twice with PBS and 400 μL of alcoholic-HCl (0.5 N HCl, 35% ethanol) was added to each well. The plates were placed on a plate shaker until all residues were solubilized. The solubilized mixtures were then transferred to a 96-well plate and the absorbances were read on a plate reader (BIO-TEK Instruments, Winooski, VT) at a wavelength of 570 nm.

4.9. NCI in vitro anti-cancer cell line screen

The human tumor cell lines used in the cancer screening panel were grown in RPMI 1640 medium containing 5% fetal bovine serum and 2 mM L-glutamine. The cells were inoculated into 96-well microtiter plates in 100 μL at plating densities ranging from 5000 to 40,000 cells/well depending on the doubling time of individual cell lines. After cell inoculation, the microtiter plates were incubated at 37 °C, 5% CO_2, 95% air in a humid atmosphere for 24 h prior to addition of experimental drugs. After 24 h, two plates of each cell line were fixed in situ by the gentle addition of 50 μL of cold 50% (w/v) TCA (final concentration, 10% TCA) and incubated for 60 min at 4 °C, to represent a measurement of the cell population for each cell line at the time of drug addition (*Tz*). Experimental drugs were solubilized in DMSO at 400-fold the desired final maximum test concentration and stored frozen prior to use. At the time of drug addition, an aliquot of frozen concentrate was thawed and diluted to twice the desired final maximum test concentration with complete medium containing 50 μg/mL gentamicin. An additional 4-fold, 10-fold, or one half log serial dilutions were made to provide a total of five drug concentrations plus control. Aliquots of 100 μL of these different drug dilutions were added to the appropriate microtiter wells already containing 100 μL of medium, resulting in the required final drug concentrations. Following drug addition, the plates were incubated for an additional 48 h. For adherent cells, the assay was terminated by the addition of cold TCA. The supernatant was discarded, and the plates were washed five times with tap water and air-dried. Sulforhodamine B (SRB) solution (100 μL) at 0.4% (w/v) in 1% acetic acid was added to each well, and plates were incubated for 10 min at room temperature. After staining, unbound dye was removed by washing five times with 1% acetic acid and the plates were air dried. Bound stain was subsequently solubilized with 10 mM trizma base, and the absorbance was read on an automated plate reader at a wavelength of 515 nm. For suspension cells, the methodology is the same except that the assay was terminated by fixing settled cells at the bottom of the wells by gently adding 50 μL of 80% TCA (final concentration, 16% TCA). Using the eight absorbance measurements [time zero, (*Tz*), control growth in the absence of drug, (C), and test growth in the presence of drug at the five concentration levels (*Ti*)], the percentage growth was calculated at each of the drug concentrations levels.

Percentage growth inhibition was calculated as:

$[(Ti - Tz)/(C - Tz)] \times 100$ for concentrations for which $Ti \geqslant Tz$,

$[(Ti - Tz)/Tz] \times 100$ for concentrations for which $Ti < Tz$.

Three dose response parameters were calculated for each experimental agent. Growth inhibition of 50% (GI_{50}) was calculated from $[(Ti - Tz)/(C - Tz)] \times 100 = 50$, which is the drug concentration resulting in a 50% lower net protein increase in the treated cells (measured by SRB staining) as compared to the net protein increase seen in the control cells. The drug concentration resulting in total growth inhibition (TGI) was calculated from $Ti = Tz$. The LC_{50} (concentration of drug resulting in a 50% reduction in the measured protein at the end of the drug treatment as compared to that at the beginning) indicating a net loss of cells following treatment was calculated from $[(Ti - Tz)/Tz] \times 100 = -50$. Values were calculated for each of these three parameters if the level of activity is reached; however, if the effect was not reached or was exceeded, the value for that parameter was expressed as greater or less than the maximum or minimum concentration tested.

4.10. NCI anti-angiogenesis screen

Cord formation assay: Matrigel (60 μL of 10 mg/mL; Collaborative Laboratories, StonyBrook, NY) was placed in each well of an ice-cold 96-well plate. The plate was allowed to sit at room temperature for 15 min then incubated at 37 °C for 30 min to permit the matrigel to polymerize. In the meantime, HUVECs were prepared in EGM-2 medium at a concentration of 2×10^5 cells/mL. The test compounds were prepared at 2× the desired concentration (5 concentration levels) in the same medium. Cells (500 μL) and 2× drug (500 μL) were mixed and 200 μL of this suspension was placed in duplicate on the polymerized matrigel. After 24 h incubation, triplicate pictures were taken for each concentration using a Bioquant Image Analysis system. Drug effect (IC_{50}) was assessed compared to untreated controls by measuring the length of cords formed and number of junctions.

Cell migration assay: Migration was assessed using a 48-well Boyden chamber and 8 μm pore size collagen-coated (10 μg/mL rat tail collagen; Collaborative Laboratories, StonyBrook, NY) polycarbonate filters (Osmonics, Inc., Minnetonka, MN). The bottom chamber wells received 27–29 μL of DMEM medium alone (baseline) or medium containing chemo-attractant (bFGF, VEGF, or Swiss 3T3 cell conditioned medium). The top chambers received 45 μL of the HUVEC cell suspension (1×10^6 cells/mL) prepared in DMEM containing 1% BSA with or without test compounds. After 5 h incubation at 37 °C, the membrane was rinsed in PBS, fixed, and stained in Diff-Quick solutions (Baxter Healthcare Co., Miami, FL). The filter was placed on a glass slide with the migrated cells facing down and cells on top were removed using a Kimwipe. The testing was performed in 4–6 replicates and five fields were counted from each well. Negative unstimulated control values were subtracted from stimulated control and drug treated values and data was plotted as mean migrated cell ± SD. IC_{50} values were calculated from the plotted data.

4.11. In vivo anti-tumor activity and toxicity

Human tumor xenografts: Twenty female, athymic nude (nu/nu) mice were purchased from Harlan Laboratories. MDA-MB-231 human breast cancer cells (10^6 cells/0.1 mL) were injected subcutaneously (sc) into the left flank of each mouse. The cells were given as a suspension in sterile MEM-alpha medium (GIBCO-BRL, Long Island, NY) containing 10% fetal bovine serum (FBS) (Mediatech, Herndon, VA), penicillin (100 units/mL) and streptomycin (100 μg/mL) and 2 mM L-glutamine. The tumors were allowed to grow for three weeks and then treated with either 5% dextrose in water (vehicle), 2, 20, or 100 mg/kg compound **14** for two weeks. The drugs were given as a sc injection near the base of the tumors. After treatment, the mice were sacrificed and the tumors were excised and weighed. The weights of the tumors from the vehicle-treated mice were compared to that of the drug treated mice and statistical analysis was performed using ANOVA. Data are presented as mean ± SE.

Toxicity: The weight of each mouse was recorded before and after treatment. At the end of the study, liver, spleen, and kidney samples were submitted to Dirk Dillehay, DVM, Emory University, for pathological examination. The maximum tolerated dose (MTD) for compound **14** was determined by the NCI as previously described.[41]

4.12. QSAR development

The 20 curcumin analogs were constructed in Macromodel 7.1,[42] optimized with the MMFF force field[43] supplemented by the GBSA/H_2O solvent model and subjected to a conformational search with the Monte Carlo method[44] to give a total of 114 conformers. Electrostatic potential atomic partial charges were applied to each of the structures using the MNDO/ESP procedure in *MOPAC 6.0*.[45] The conformers were superimposed by means of *FlexS* in *Sybyl 6.7*[46] with the structure of **14** as template to give the pharmacophore. A single pdb file containing all the conformers was constructed with PrGen 2.1[47] and then submitted to *Quasar 3.5* for QSAR analysis.[36] For the training set of 14 compounds, the iterative Quasar procedure evolved to the quasi-atomistic binding site depicted in Figure 3 with $r^2 = 0.85$ and a cross-validated r^2 (i.e., q^2) = 0.83. The RMS deviation is 0.24 kcal/mol with a maximum deviation of 0.64 kcal/mol. These values arise by averaging over the best 300 models provided by Quasar's genetic search algorithm. The average receptor model is depicted in Figure 3. When applied to a test set of five additional analogs, a predictive r^2 (i.e., p^2) = 0.71 was obtained with an RMS deviation of 0.44 kcal/mol and a maximum deviation of 0.72 kcal/mol. The QSAR correlation combining both training and test sets is depicted in Figure 4. The individual error bars arise by averaging the maximum and minimum deviations in kcal/mol for each ligand over the 300 best models. To assure that the correlation is not fortuitous, we performed three scramble tests on the data. The average for the three is

$p^2 = -0.30$, demonstrating the robustness of the plot in Figure 4.

Acknowledgements

This work was supported by grants from the Department of Health and Human Services (CA82995) and the US Department of Defense, the Division of US Army (DAMD17-00-1-0241), and a contract with the George Washington University Medical Center. A portion of the studies described herein were also supported with Federal funds from the National Cancer Institute, National Institutes of Health, under Contract N01-CM-5600. Mention of trade names or commercial products in this publication does not imply endorsement by the US Government.

References and notes

1. Mehta, K.; Pantazis, P.; McQueen, T.; Aggarwal, B. B. *Anti-Cancer Drugs* **1997**, *8*, 470–481.
2. Kuo, M. L.; Huang, T. S.; Lin, J. K. *Biochim. Biophys. Acta* **1996**, *1317*, 95–100.
3. Jee, S. H.; Shen, S. C.; Tseng, C. R.; Chiu, H. C.; Kuo, M. L. *J. Invest. Dermatol.* **1998**, *111*, 656–661.
4. Kawamori, T.; Lubet, R.; Steele, V. E.; Kelloff, G. J.; Kaskey, R. B.; Rao, C. V.; Reddy, B. S. *Cancer Res.* **1999**, 597–601.
5. Singletary, K.; MacDonald, C.; Iovinelli, M.; Fisher, C.; Wallig, M. *Carcinogenesis* **1998**, *19*, 1039–1043.
6. Ruby, A. J.; Kuttan, G.; Babu, K. D.; Rajasekeharan, K. N.; Kuttan, R. *Cancer Lett.* **1995**, *94*, 79–83.
7. Kuttan, R.; Bhanumathy, P.; Nirmala, K.; George, M. C. *Cancer Lett.* **1985**, *29*, 197–202.
8. Arbiser, J. A.; Klauber, N.; Rohan, R.; van Leeuwen, R.; Huang, M. T.; Fisher, C.; Flynn, E.; Byers, H. R. *Mol. Med.* **1998**, *4*, 376–383.
9. Thaloor, D.; Singh, A. K.; Sidhu, G. S.; Prasad, P. V.; Kleinman, H. K.; Maheshwari, R. K. *Cell Growth Differentiation* **1998**, *9*, 305–312.
10. (a) Kelloff, G.; Crowell, J.; Hawk, E. *J. Cell. Biochem.* **1996**, *26*, 72–85; (b) Aggarwal, B. B.; Kumar, A.; Bharti, A. C. *Anticancer Res.* **2003**, *23*, 363–398.
11. Shoba, G.; Joy, D.; Joseph, T., et al. *Planta Med.* **1998**, *64*, 353–356.
12. Anto, R. J.; George, J.; Dinesh Babu, K. V.; Rajasekeharan, K. N.; Kuttan, R. *Mutation Res.* **1996**, *370*, 127–131.
13. Dinkova-Kostova, A. T.; Abeygunawardana, C.; Talalay, P. *J. Med. Chem.* **1998**, *41*, 5287–5296.
14. Markaverich, B. M.; Schauweker, T. H.; Gregory, R. R.; Varma, M.; Kittrell, F. S.; Medina, D.; Varma, R. S. *Cancer Res.* **1992**, *52*, 2482–2488.
15. Dinkova-Kostova, A. T.; Abeygunawardana, C.; Talalay, P. *J. Med. Chem.* **1998**, *41*, 5287–5296.
16. Artico, M.; Di Santo, R.; Costi, R.; Novellino, E.; Greco, G.; Massa, S.; Tramontano, E.; Marongui, M.; De Montis, A.; La Colla, P. *J. Med. Chem.* **1998**, *41*, 3948–3960.
17. El-Subbagh, E. I.; Abu-Zaid, S. M.; Mahran, M. A.; Badria, F. A.; Al-Obaid, A. M. *J. Med. Chem.* **2000**, *43*, 2915–2921.
18. Dimmock, J. R.; Vashishtha, S. C.; Quail, J. W.; Pugazhenthi, U.; Zimpel, Z.; Sudom, A. M.; Allen, T. M.; Kao, G. Y.; Balzarini, J.; De Clercq, E. *J. Med. Chem.* **1999**, *42*, 1358–1366.
19. Dimmock, J. R.; Kandepu, N. M.; Nazarali, A. J.; Kowalchuk, T. P.; Motaganahalli, N.; Quail, J. W.; Mykytiuk, P. A.; Audette, G. F.; Prasad, L.; Perjési, P.; Allen, T. M.; Santos, C. L.; Szydlowski, J.; De Clercq, E.; Balzarini, J. *J. Med. Chem.* **1998**, *41*, 4012–4020.
20. Dimmock, J. R.; Kumar, P.; Nazarali, A. J.; Motaganahalli, N.; Kowalchuk, T. P.; Beazeley, M. A.; Quail, J. W.; Oloo, E. O.; Allen, T. M.; Szydlowski, J.; De Clercq, E.; Balzarini, J. *Eur. J. Med. Chem.* **2000**, *35*, 967–977.
21. Dimmock, J. R.; Padmanilayam, M. P.; Puthucode, R. N.; Nazarali, A. J.; Motaganahalli, N.; Zello, G. A.; Quail, J. W.; Oloo, E. O.; Kraatz, H.-B.; Prisciak, J. A.; Allen, T. M.; Santos, C. L.; Balzarini, J.; De Clercq, E.; Manavathu, E. K. *J. Med. Chem.* **2001**, *44*, 586–593.
22. McGookin, A.; Heilbron, I. M. *J. Chem. Soc.* **1924**, *125*, 2105–2199.
23. Nauduri, D.; Reddy, G. B. S. *Chem. Pharm. Bull.* **1998**, *46*, 1254–1260.
24. Artico, M.; DiSanto, R.; Costi, R.; Novellino, E.; Greco, G.; Massa, S.; Tramontano, E.; Marongiu, M. E.; DeMontis, A.; LaColla, P. *J. Med. Chem.* **1998**, *41*, 3948–3960.
25. Jennings, W. P.; McGookin, A. *J. Chem. Soc.* **1934**, 1741–1742.
26. Sardjiman, S. S.; Reksohadiprodjo, M. S.; Hakim, L.; van der Goot, H.; Trimmerman, H. *Eur. J. Med. Chem. Chim. Ther.* **1997**, *32*, 625–630.
27. Borsche, W.; Geyer, A. *Justus Liebigs Ann. Chem.* **1912**, *393*, 29–60.
28. Kraft, D.; Cacciapaglia, R.; Boehmer, V.; El-Fadl, A. A.; Haekema, S. *J. Org. Chem.* **1992**, *57*, 826–834.
29. McElvain, S. M.; McMahon, R. E. *J. Am. Chem. Soc.* **1949**, *71*, 901–906.
30. Grever, M.; Schepartz, S.; Chabner, B. *Semin. Oncol.* **1992**, *19*, 622–638.
31. Monks, A.; Scudiero, D.; Skehan, P., et al. *J. Natl. Cancer Inst.* **1991**, *83*, 757–766.
32. Boyd, M.; Paull, K. *Drug Dev. Res.* **1995**, *34*, 91–109.
33. Zhang, S. Z.; Lipsky, M. M.; Trump, B. F.; Hsu, I. C. *Cell Biol. Toxicicol.* **1990**, *6*, 219–234.
34. Arbiser, J. L.; Moses, M. A.; Fernandez, C. A.; Ghiso, N.; Cao, Y.; Klauber, N.; Frank, D.; Brownlee, M.; Flynn, E.; Parangi, S.; Byers, H. R.; Folkman, J. *Proc. Natl. Acad. Sci.* **1997**, *94*, 861–866.
35. Yanase, T.; Tamura, M.; Fujita, K.; Kodama, S.; Tanaka, K. *Cancer Res.* **1993**, *53*, 2566–2570.
36. Vedani, A.; Dobler, M. *5D-QSAR: J. Med. Chem.* **2002**, *45*, 2139–2149.
37. While only 14 curcuminoid compounds are listed in Tables 2–6, for the purpose of QSAR model-building the tabulated values were supplemented by six additional datapoints from the same compound class; Lu, Y. Emory University, private communication.
38. Mora, P. T.; Szeki, T. *J. Am. Chem. Soc.* **1950**, *72*, 3009–3013.
39. Tanaka, T.; Miyaguchi, M.; Mochisuki, R. K.; Tanaka, S.; Okamota, M. *Heterocycles* **1987**, *25*, 463–484.
40. Baeyer, A.; Villiger, V. *Chem. Ber.* **1902**, *35*, 3013–3033.
41. Hollingshead, M. G.; Alley, M. C.; Camalier, R. F.; Abbott, B. J.; Mayo, J. G., et al. *Life Sci.* **1995**, *57*, 131–141.
42. Mohamadi, F.; Richards, N. G. J.; Guida, W. C.; Liskamp, R.; Lipton, M.; Caufield, C.; Chang, G.;

Hendrickson, T.; Still, W. C. *J. Comput. Chem.* **1990**, *11*, 440–467.
43. Halgren, T. A. *J. Comp. Chem.* **1996**, *17*, 490–641.
44. Chang, G. G.; Guida, W. C.; Still, W. C. *J. Am. Chem. Soc.* **1989**, *111*, 4379–4386.
45. Stewart, J. P. P. *J. Comp.-Aided Mol. Des.* **1990**, *4*, 1–5.
46. Lemmen, C.; Lengauer, T. *J. Comp.-Aided Mol. Des.* **1997**, *11*, 357–368.
47. Zbinden, P.; Dobler, M.; Folkers, G.; Vedani, A. *Quant. Struct.-Act. Relat.* **1998**, *17*, 122–130.
48. (a) Paull, K. D.; Shoemaker, R. H.; Hodes, L.; Monks, A.; Scudiero, D. A.; Rubenstein, L.; Plowman, J.; Boyd, M. R. *J. Natl. Cancer Inst.* **1989**, *81*, 1088–1092; (b) Development Therapeutics Program NCI/NIH. COMPARE Methodology.http://dtp.nci.nih.gov/docs/compare/compare_methodology.html.